Systematics of Ni and Co in olivine from planetary melt systems: Lunar mare basalts

J.J. Papike,* G.W. Fowler, C.T. Adcock, and C.K. Shearer

Institute of Meteoritics, Department of Earth and Planetary Sciences, University of New Mexico, Albuquerque, New Mexico 87131-1126, U.S.A.

Abstract

The systematics of Co and Ni in olivine from six Apollo 12 olivine basalts were studied by SIMS techniques and correlated with major and minor element data obtained with the electron microprobe. Our results, together with previous studies, demonstrate that one of these basalts (12009) was extruded, as a liquid, onto the lunar surface and was parental to five other cumulates (12075, 12020, 12018, 12040, and 12035). The concentrations of Ni in zoned olivine phenocrysts behave as expected for a highly compatible element with initial estimated D_{Ni} = 9.9. On the other hand, Co concentrations in olivine vary hardly at all and show flat patterns across crystals that retain normal zoning trends for Mg, Fe, Mn, and Ni. The explanation for this behavior is not that $D_{Co} \approx 1$ (our estimated D_{Co} = 4) or that Co zoning has been erased by rapid diffusion of Co compared to the other elements (e.g., Mg and Fe) that still show normal zoning. The explanation for the behavior, as originally suggested by Kohn et al. (1989), is that the increase in D_{Co} with crystallization exactly balances the depletion of Co in the melt. This decoupling of the behavior of Ni and Co in olivine results in significant increases in Co/Ni with crystallization.

Introduction

Olivine can be an important and early crystallizing phase in lunar mare basalts. The Apollo 12 olivine basalts are an especially interesting suite of samples because they may represent one or more fractionation series and also experienced different cooling rates (e.g., Papike et al. 1976; Neal et al. 1994a, 1994b). Olivine is an important recorder of basalt evolution and the Fo content of early crystallizing olivine cores, together with the Fe-Mg exchange coefficient (K_D: e.g., Jones 1995), can be used to predict the Mg′[= Mg/(Mg+Fe) atomic] of equilibrium melts. If the actual bulk composition of a basalt sample has the Mg′ predicted from the olivine, then it appears that the olivine crystallized from the melt represented by the bulk sample composition and is not cumulus. We developed SIMS techniques for analyzing Co and Ni in olivine (Papike et al. 1995) and now use these techniques to study the Co-Ni systematics in olivine from mare basalts. We began with six samples representative of the Apollo 12 olivine basalts. We looked first at the distribution of Co and Ni between the most Mg-rich olivine cores and the melt. If the measured Mg′ of the bulk rock and the Mg′ predicted from the olivine are the same, then the Co, Ni of the bulk sample should also agree with that calculated from olivine.

Considerable work has been done on the Apollo 12 olivine basalts. Green et al. (1971) conducted experimental phase equilibrium studies of lunar sample 12009. This is a rapidly quenched basalt with microphenocrysts of

olivine and spinel in a cryptocrystalline matrix. Green et al. concluded that this rock represents the original liquid because the most magnesian olivine core compositions are the same as the experimentally produced liquidus olivines. Donaldson et al. (1975) conducted experiments designed to determine the cooling history of the Apollo 12 olivine basalts. They found that mineral chemistry, crystal shapes, grain sizes, and textures are related systematically to cooling rate and degree of supercooling. At linear cooling rates of ≤40 °C/h, the texture is porphyritic with larger olivine crystals set in a groundmass of finer-grained pyroxene, plagioclase, and ilmenite. Walker et al. (1976a) studied the phase equilibria and cooling rate of Apollo 12 olivine basalt 12002. They found that the partitioning of Fe^{2+} and Mg between olivine and liquid (K_D = 0.33) is independent of cooling rate (0.5–2000 °C/h), temperature (1325–600 °C), and pressure (0–12 Kb).

A paper by Walker et al. (1976b) concerned with the differentiation of an Apollo 12 picrite magma formed the basis for the present study. Walker et al. (1976b) found that the Apollo 12 olivine basalt suite shows a strong positive correlation of grain size with normative olivine content. This correlation is interpreted to mean that the suite of samples represents the basal portion of a cooling unit that differentiated by simple olivine settling. The grain size of plagioclase observed in the coarsest samples indicates the cooling unit may have been as much as 30 m thick. The proportion of olivine observed in each sample of the suite is quantitatively internally consistent with simple olivine settling in a magma body of this size, which has the composition of the chilled margin (=
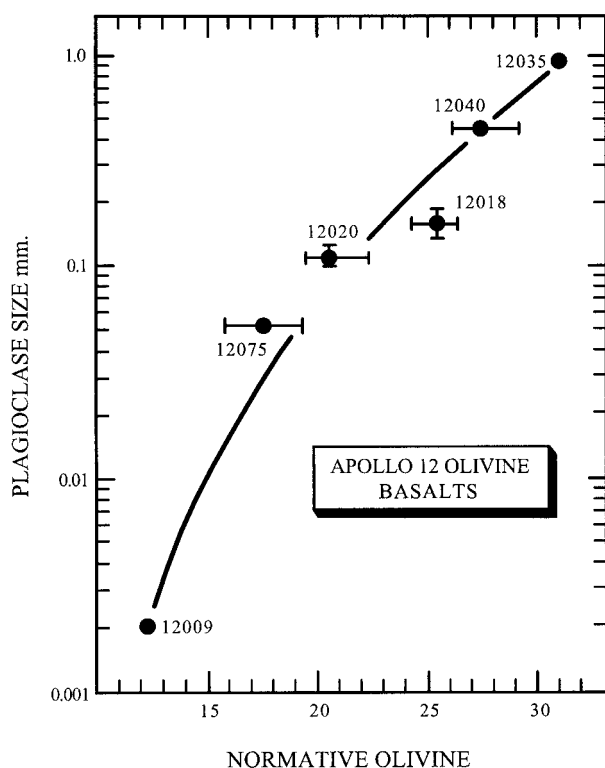
FIGURE 1. Plagioclase grain size vs. amount of normative olivine in Apollo 12 Olivine basalts (after Walker et al. 1976b).

12 009). In this study, normative olivine abundance is the principal index of differentiation and plagioclase grain size is the principal feature related to cooling history. Figure 1 (adapted from Walker et al. 1976b) shows this relationship for six of the Apollo 12 olivine basalts, and Figure 2 is a series of backscattered electron (BSE) images of the same samples. These relationships indicate that 12009 has the composition of the initial melt, and 12035 is the most evolved cumulate. These authors tabulated the compositions of the most Mg-rich olivine cores and found that 12009, 12075, 12020, and 12018 have compositions ($\sim Fo_{75-76}$) that indicate cumulus olivine in 12075, 12020, and 12018 could have originated in a melt of 12009 composition. However, the coarsest-grained cumulates, 12040 and 12035, have olivine core compositions of Fo_{63-67}, indicating that the cores either reequilibrated with or nucleated from more evolved melt.

An additional factor in the experimental design of this study was inspired by a paper by Kohn et al. (1989) in which these authors reported elemental zoning trends in olivine phenocrysts from an Mg-rich andesite. They found that Ni had the expected zoning trend for a compatible element (e.g., it follows Mg), but Co showed almost no zoning. We will also address this issue and give a possible explanation below.

The bulk-rock compositions (major elements plus Co and Ni) are presented in Table 1 and were obtained from Lofgren and Lofgren (1981).

ANALYTICAL AND COMPUTATIONAL TECHNIQUES

Analytical approach

Major and minor elements were analyzed on a JEOL 733 Superprobe, equipped with a BSE detector, five wavelength spectrometers, and a thin-window energy-dispersive spectrometer controlled by an Oxford Link eXL II analyzer system. Olivine compositions were measured by wavelength-dispersive spectrometry, with peak counting times ranging from 20 s for major elements to 40 s for minor elements at a beam current of 20 nA. All analyses were conducted at 15 kV, and ZAF corrections were applied to the analyses. A beam size of 1 μm was used.

Ion microprobe analyses of olivine were conducted using a Cameca IMS 4f instrument. The olivine analyses involved repeated cycles of peak counting on $^{55}Mn^+$, $^{59}Co^+$, $^{60}Ni^+$, and $^{30}Si^+$ as a reference species. The analytical procedure included counting on a background position to monitor detection noise. Absolute concentrations of each element were calculated using empirical relationships of measured peak/$^{30}Si^+$ ratios (normalized to known SiO_2 content) to element concentrations as derived from daily calibration measurements of the following olivine standards: PM150, which contains 1095 ppm Mn, 140 ppm Co, and 3170 ppm Ni; SCKA, which contains 1065 ppm Mn, 143 ppm Co, and 2950 ppm Ni; and MARJ, which contains 2200 ppm Mn, 7 ppm Co, and 34 ppm Ni.

Analyses were made by bombardment of the sample with primary O^- ions accelerated through a nominal potential of 10 kV. A primary ion current of 30–40 nA was focused on the sample over a spot diameter of 25–35 μm. Sputtered secondary ions were energy filtered using sample offset voltages of −105 V, and an energy window of ±25 V, to eliminate effectively most isobaric interferences (Shimizu et al. 1978). Peak counting times were varied to optimize precision. For olivine analyses, a precision of better than 2% was achieved.

All ion microprobe analyses were conducted at locations analyzed previously with the electron microprobe, and the SiO_2 concentrations determined by EMP were used in reducing the SIMS data. Inclusion of contaminating phases in the SIMS analyses was avoided by selecting optically clean olivine grains and by mass imaging of major elements before and after each spot SIMS analysis.

Modeling approach

Our overall approach to evaluating the crystallization history of the olivine in the Apollo 12 olivine basalts was two-fold: (1) major-element modeling using computational evaluations of equilibrium and fractional crystallization, and (2) trace-element modeling of crystallization using phase relations and melt compositions calculated in the first step and integrating changing $D_{Ni,Co}$ during basalt crystallization.

The major-element modeling of the equilibrium and fractional crystallization of Apollo 12 olivine basalts was
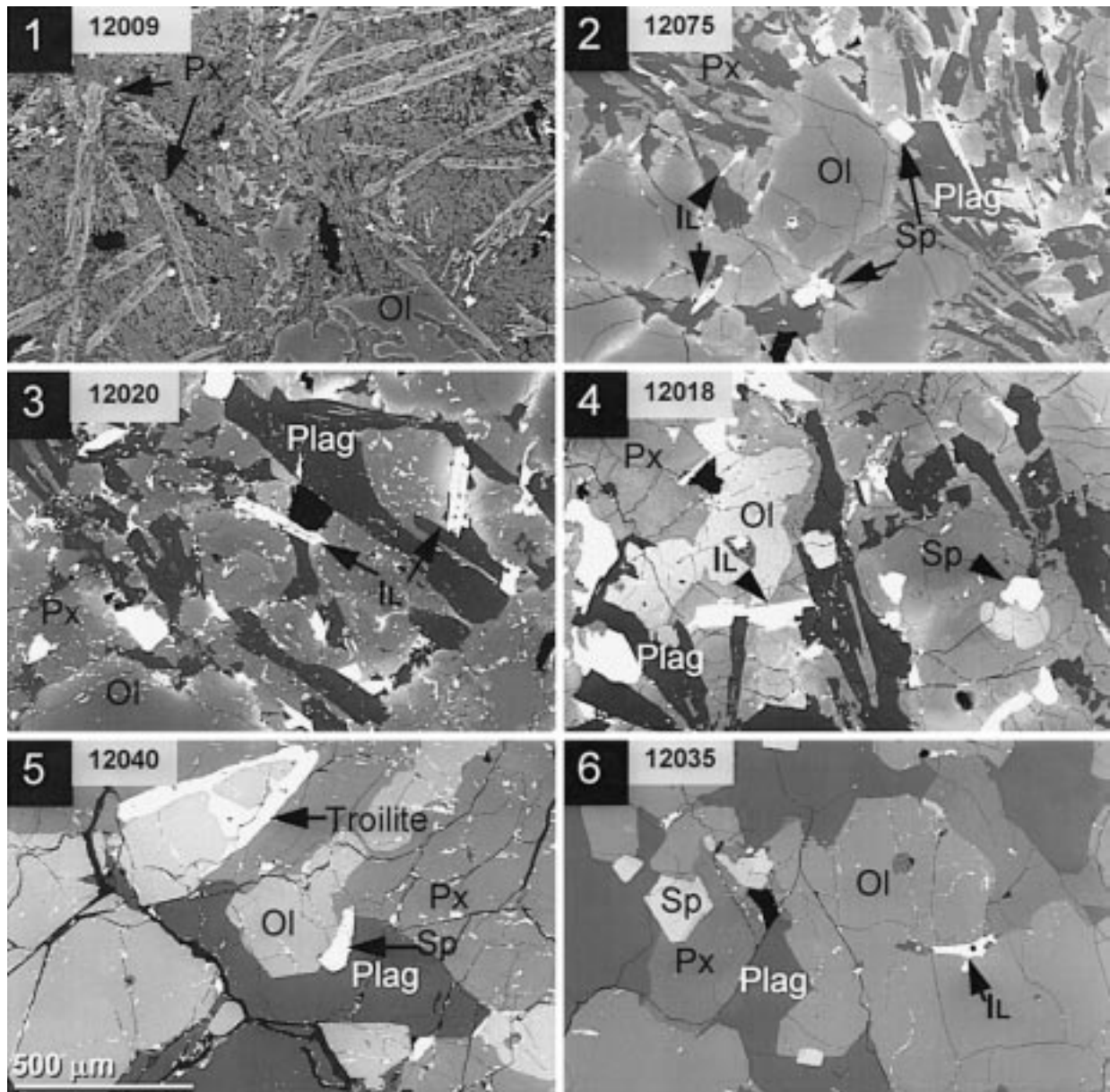
FIGURE 2. A series of BSE images for six Apollo 12 olivine basalts. The scale for all images is the same as noted for 12040.

done using the MELTS program (Ghiorso and Sack 1995). MELTS works by the parameterization of multi-component solid solutions and magmatic liquids to predict mineral-melt equilibria. We used an AIX 4.1 version of MELTS assembled on the University of New Mexico computer system by Mark Ghiorso in 1996. In our calculations, we assumed that the bulk composition represented by sample 12009 (Table 1) approached a parental melt composition for the Apollo 12 olivine basalts. Conditions under which the MELTS calculations were made are as follows: temperatures ranged from 1400 to 900 °C, pressure equaled 1 atm, and oxygen fugacities were defined by the iron-wustite (IW) buffer. Lunar basalts crys-

tallized at the IW buffer to 1–2 log units below the IW buffer (BVSP 1981). Both equilibrium and fractional crystallization processes were modeled using MELTS. These calculations provided us with the sequence of crystallization, evolving melt and mineral phase compositions, percent crystallization, and temperature.

Using the melt compositions calculated from MELTS, we calculated changing $D_{Ni}^{olivine}$ over the temperature interval of olivine crystallization from the relationship defined by Hart and Davis (1978) (Fig. 3):

$$D_{Ni}^{olivine} = (124.13/MgO_{Melt}) - 0.897.$$

More recent formulations of the relationship between

TABLE 1. Chemistry of Apollo 12 olivine basalts

Sequence wt%	1 12009	2 12075	3 12020	4 12018	5 12040	6 12035
SiO_2	45.03	44.93	44.57	43.9	43.88	43.17
TiO_2	2.90	2.69	2.76	2.59	2.45	2.28
Al_2O_3	8.59	8.39	7.77	7.97	7.27	8.03
FeO	21.03	20.47	20.98	20.96	21.09	22.20
MnO	0.28	0.27	0.27	0.27	0.27	0.29
MgO	11.55	13.86	14.40	15.23	16.45	15.49
CaO	9.42	8.59	8.60	8.33	8.01	8.08
Na_2O	0.23	0.27	0.22	0.22	0.17	0.21
K_2O	0.06	0.06	0.06	0.05	0.05	0.05
P_2O_5	0.07	0.12	0.08	0.07	0.06	0.06
S	0.06	–	0.06	0.05	0.04	0.05
Cr_2O_3	0.55	0.60	0.61	0.62	0.63	0.49
Total	99.77	100.25	100.38	100.26	100.37	100.40
Mg′	0.494	0.547	0.550	0.564	0.581	0.554
ppm						
Ni	52	63	50	55	40	33
Co	49	61	61	58	61	53
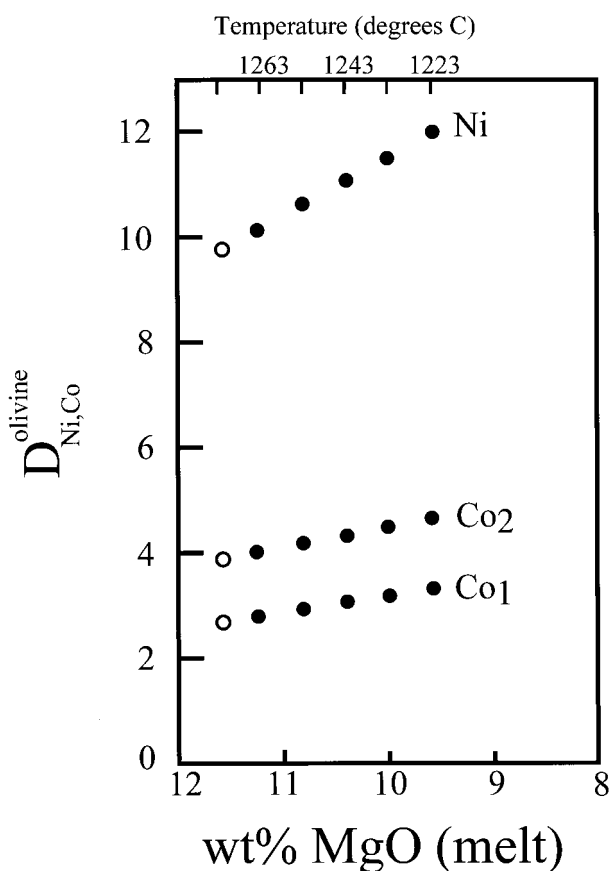
FIGURE 3. The variation in $D_{Ni,Co}^{olivine}$ during olivine crystallization in 12009. The melt composition and temperature were calculated using MELTS. $D_{Ni}^{olivine}$ was calculated using the relationship defined by Hart and Davis (1978): $D_{Ni}^{olivine} = (124.13/MgO) -0.897$. $D_{Co}^{olivine}$ was approximated using the relationship between $D_{Ni}^{olivine}$ and $D_{Co}^{olivine}$ formulated by Jones (1995, personal communication): $D_{Co_1}^{olivine} = 0.235 D_{Ni} + 0.476$. $D_{Co_2}^{olivine}$ was approximated using the measured ratio $Co^{olivine}/Co^{whole\ rock}$ and the variability in D_{Co} observed in D_{Co_1}. Open symbols represent the estimated D value for olivine just prior to olivine crystallization.

$D_{Ni}^{olivine}$ and melt composition (Kinzler et al. 1990) demonstrated that the equation of Hart and Davis (1978) predicted $D_{Ni}^{olivine}$ higher than measured for melt compositions at high MgO and high FeO. Fortunately, at the melt compositions used here (8–12 wt% MgO), the Hart and Davis (1978) formulation is similar to that of Kinzler et al. (1990). The result of the formulation differs from that of Jones (1995) (9.8 compared to 7.4), but was selected because it also agreed closely with our measured value. We then calculated two sets of values for $D_{co}^{olivine}$. The first values of $D_{co}^{olivine}$ (D_{Co_1}) was calculated for each D_{Ni} olivine/melt using the formulation of Jones (1995):

$$D_{co}^{olivine} = 0.235\ D_{Ni}^{olivine} + 0.476.$$

We also calculated the $D_{co}^{olivine}$ based on the Co content of the olivine core and bulk composition of sample 12009 (D_{Co_2}). The change in this $D_{co}^{olivine}$ with temperature was set to be equivalent to the variation observed in D_{Co_1}. Based on the results from MELTS and the calculated $D_{Ni,Co}^{olivine}$, we determined the behavior of Co and Ni in the melt and olivine during the crystallization of a basaltic melt with a composition equal to 12009. The concentrations of Co and Ni in the melt and olivine were calculated at 10 °C intervals for fractional and equilibrium crystallization models.

RESULTS AND DISCUSSION

The EMP and SIMS (Mn, Co, Ni) data are tabulated in Table 2. Figure 4 illustrates the typical zoning behavior for Ni, X_{Fe} [Fe/(Fe + Mg) (atomic)], Mn, and Co. Nickel behaves as expected for a compatible element and decreases as X_{Fe} and Mn increases (both Fe and Mn are incompatible). However, Co is interesting because the zoning pattern is nearly flat. Kohn et al. (1989) observed similar behavior for Co in olivine phenocrysts from an Mg-rich andesite. Kohn et al. estimated that olivine D_{Co} = 4.2, so the flat zoning trends cannot be explained by a $D \approx 1$. Kohn et al. stated that the lack of Co zoning could be explained in two ways: (1) Co diffusion in olivine is rapid compared with Mg, Fe, Ni, or Mn; or (2) an in-

TABLE 2. Chemistry of olivine from Apollo 12 olivine basalts

Analysis	12009,14					12075,28								12020,13					
	Core 1	2	3	Rim 4	Rim G-2	Core 1	2	3	4	Rim 5	Rim 1	2	3	4	Core 5	6	7	8	Rim 9
SiO$_2$	37.62	38.22	37.75	37.34	36.15	37.95	37.86	37.74	37.43	34.87	36.76	37.71	38.08	37.93	37.96	38.21	37.49	37.56	36.88
Al$_2$O$_3$	0.00	0.00	0.00	0.00	0.07	0.00	0.00	0.00	0.00	0.00	0.06	0.06	0.06	0.06	0.09	0.05	0.06	0.06	0.07
TiO$_2$	0.06	0.06	0.06	0.08	0.18	0.00	0.00	0.00	0.00	0.00	0.06	0.07	0.07	0.07	0.05	0.08	0.05	0.09	0.07
Cr$_2$O$_3$	0.42	0.41	0.39	0.41	0.38	0.36	0.36	0.35	0.35	0.27	0.43	0.49	0.50	0.50	0.43	0.45	0.52	0.47	0.46
MgO	37.51	37.72	36.46	33.83	29.80	37.59	37.23	36.56	36.18	24.30	33.08	36.30	37.64	37.89	37.65	37.19	35.91	35.58	33.21
FeO	22.01	22.83	23.58	26.71	32.16	22.60	23.07	23.42	24.41	38.63	28.12	24.10	23.08	22.69	22.89	23.00	24.42	25.02	27.91
MnO	0.17	0.18	0.19	0.24	0.40	0.11	0.14	0.14	0.15	0.31	0.36	0.31	0.26	0.30	0.28	0.29	0.34	0.33	0.34
CaO	0.27	0.24	0.23	0.25	0.38	0.21	0.21	0.23	0.22	0.24	0.25	0.27	0.24	0.24	0.27	0.28	0.27	0.26	0.28
Total	98.06	99.66	98.66	98.86	99.52	98.82	98.87	98.44	98.74	98.73	99.12	99.31	99.93	99.68	99.62	99.55	99.06	99.37	99.22
%Fo	75	75	73	69	62	75	74	74	73	53	68	73	74	75	75	74	72	72	68
Formula proportions of cations based on 4 O atoms																			
Si	0.999	1.001	1.003	1.006	0.996	1.001	1.001	1.004	0.998	1.001	0.996	0.998	0.996	0.994	0.996	1.003	0.997	0.999	0.997
Al	0.000	0.000	0.000	0.000	0.002	0.000	0.000	0.000	0.000	0.000	0.002	0.002	0.002	0.002	0.003	0.002	0.002	0.002	0.002
Σ	0.999	1.001	1.003	1.006	0.998	1.001	1.001	1.004	0.998	1.001	0.998	1.000	0.998	0.996	0.999	1.005	0.999	1.001	0.999
Ti	0.001	0.001	0.001	0.001	0.004	0.000	0.000	0.000	0.000	0.002	0.001	0.001	0.001	0.001	0.001	0.002	0.001	0.002	0.001
Cr	0.009	0.008	0.008	0.009	0.008	0.008	0.008	0.007	0.007	0.006	0.009	0.010	0.010	0.010	0.009	0.009	0.011	0.010	0.010
Mg	1.485	1.473	1.444	1.358	1.223	1.479	1.467	1.450	1.438	1.040	1.336	1.433	1.468	1.480	1.472	1.455	1.424	1.410	1.338
Fe	0.489	0.500	0.524	0.601	0.741	0.499	0.510	0.521	0.544	0.928	0.637	0.534	0.505	0.497	0.502	0.505	0.543	0.556	0.631
Mn	0.004	0.004	0.004	0.005	0.009	0.002	0.003	0.003	0.003	0.008	0.008	0.007	0.006	0.007	0.006	0.006	0.008	0.007	0.008
Ca	0.008	0.007	0.006	0.007	0.011	0.006	0.006	0.007	0.006	0.007	0.007	0.008	0.007	0.007	0.008	0.008	0.008	0.007	0.008
Σ	1.996	1.993	1.987	1.982	1.996	1.994	1.994	1.988	1.998	1.991	1.998	1.993	1.997	2.002	1.998	1.985	1.995	1.992	1.996
Mn ppm	2713	2812	2956	2970	3098	2760	2911	2977	3139	3222	3751	3398	2966	2777	2733	2754	2696	2818	2867
Co ppm	194	196	200	201	201	193	195	194	201	178	197	202	197	195	193	194	190	193	191
Ni ppm	512	514	510	466	390	499	467	444	433	357	245	350	455	481	508	488	488	486	451

Analysis	12018,7						12040,44						12035,63					
	Core 1	2	3	4	5	Rim 6	Core 1	2	3	4	5	Rim 6	Core 1	2	3	4	5	Rim 6
SiO$_2$	35.96	36.13	36.39	36.39	35.43	34.45	35.89	35.81	35.69	35.21	34.41	33.78	35.52	34.74	35.28	35.19	34.94	35.02
Al$_2$O$_3$	0.05	0.06	0.06	0.07	0.06	0.05	0.10	0.06	0.06	0.06	0.06	0.07	0.06	0.13	0.04	0.04	0.05	0.05
TiO$_2$	0.10	0.11	0.10	0.12	0.10	0.14	0.11	0.12	0.12	0.12	0.13	0.15	0.12	0.14	0.11	0.11	0.11	0.15
Cr$_2$O$_3$	0.20	0.15	0.19	0.22	0.21	0.16	0.18	0.19	0.17	0.19	0.18	0.15	0.22	0.23	0.20	0.18	0.20	0.18
MgO	28.82	29.52	30.32	30.36	26.68	22.56	25.45	25.95	26.14	24.81	21.38	18.35	26.77	27.12	26.72	26.37	25.72	25.07
FeO	33.87	32.77	32.08	31.73	36.25	41.75	35.95	34.30	34.31	35.53	40.36	43.36	35.89	36.54	36.64	36.81	37.04	38.10
MnO	0.39	0.38	0.38	0.36	0.42	0.47	0.45	0.42	0.44	0.45	0.44	0.54	0.45	0.44	0.46	0.43	0.46	0.46
CaO	0.28	0.28	0.26	0.26	0.27	0.34	0.31	0.28	0.32	0.29	0.35	0.32	0.34	0.32	0.17	0.31	0.30	0.29
Total	99.67	99.40	99.78	99.51	99.42	99.92	98.44	97.13	97.25	96.66	97.36	96.72	99.37	99.66	99.62	99.44	98.82	99.32
%Fo	60	62	63	63	57	49	56	57	58	55	49	43	57	57	57	56	55	54
Formula proportions of cations based on 4 O atoms																		
Si	0.996	0.998	0.997	0.998	0.997	0.993	1.016	1.020	1.016	1.016	1.011	1.017	0.998	0.979	0.993	0.994	0.995	0.996
Al	0.002	0.002	0.002	0.002	0.002	0.002	0.003	0.002	0.002	0.002	0.002	0.002	0.002	0.004	0.001	0.001	0.002	0.002
Σ	0.998	1.000	0.999	1.000	0.999	0.995	1.019	1.022	1.018	1.018	1.013	1.019	1.000	0.983	0.994	0.995	0.997	0.998
Ti	0.002	0.002	0.002	0.002	0.002	0.003	0.002	0.003	0.003	0.003	0.003	0.003	0.003	0.003	0.002	0.002	0.002	0.003
Cr	0.004	0.003	0.004	0.005	0.005	0.004	0.004	0.004	0.004	0.004	0.004	0.004	0.005	0.005	0.004	0.004	0.005	0.004
Mg	1.190	1.216	1.239	1.242	1.119	0.969	1.074	1.101	1.109	1.067	0.937	0.824	1.121	1.139	1.121	1.110	1.092	1.063
Fe	0.785	0.757	0.735	0.728	0.853	1.006	0.851	0.817	0.816	0.857	0.992	1.092	0.843	0.861	0.862	0.869	0.882	0.907
Mn	0.009	0.009	0.009	0.008	0.010	0.011	0.011	0.010	0.011	0.011	0.012	0.010	0.011	0.010	0.010	0.010	0.011	0.011
Ca	0.008	0.008	0.008	0.008	0.008	0.010	0.009	0.009	0.010	0.009	0.011	0.010	0.010	0.010	0.005	0.009	0.009	0.009
Σ	1.998	1.995	1.997	1.993	1.997	2.003	1.951	1.944	1.953	1.951	1.959	1.947	1.993	2.028	2.004	2.004	2.001	1.997
Mn ppm	3631	3653	3651	3856	4293	5005	4633	4558	4752	5171	5477	5569	4472	4389	4577	4703	4717	4958
Co ppm	222	201	193	195	194	188	203	202	200	207	209	208	197	198	194	200	206	213
Ni ppm	302	287	300	325	283	184	146	144	132	107	98	92	129	124	111	121	110	106
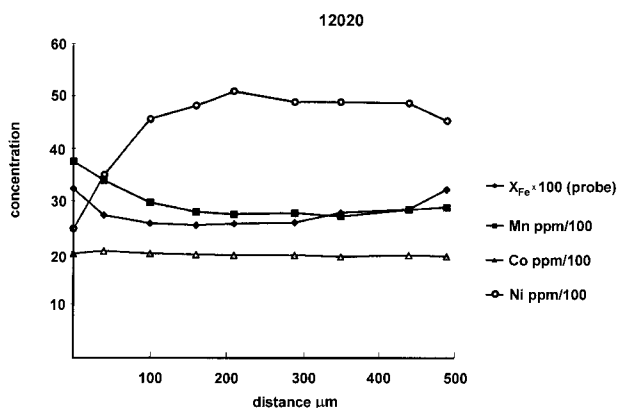
FIGURE 4. Elemental zoning trends across an olivine phenocryst in Apollo 12 olivine basalt 12020.

FIGURE 5. Systematics of Co (5a), Ni (5b), and Co/Ni (5c) vs. Mn and Fo contents of olivine in six Apollo 12 olivine basalts.

crease in D_{Co} with increasing crystallization exactly balances the depletion of Co in the melt. Kohn et al. discount the first explanation because it has been shown that the order of diffusion rates is Mn > Fe = Mg > Co > Ni (Morioka 1980 1981; Miyamoto and Takeda 1983).

Using the olivine core composition (Ni = 514 ppm, Co = 196 ppm, Table 2) and the bulk rock composition of 12009 as an estimate of the corresponding melt composition (Ni = 52 ppm, Co = 49 ppm, Table 1), we calculated D_{Ni} = 9.9 and D_{Co} = 4.0. This compares to calculated values of D_{Ni} = 9.8 using the approach of Hart and Davis (1978), and D_{Co} = 2.8 using the relationship of Jones (1995).

Figure 5 shows the variation of Co, Ni, and Co/Ni vs. Mn (or olivine Fo values). What is clear from these diagrams is that Ni behaves as a highly compatible element but Co does not, and Co/Ni decoupling leads to a significant increase in Co/Ni ratios in olivine with crystallization. It is also apparent from Figure 5 that the two most evolved (lower Fo contents in olivine cores) and the most slowly cooled (coarsest grain sizes) cumulates, 12035 and 12040, behave differently from the other four samples. This is probably due to the fact that the olivine phenocrysts nucleated in more evolved melts (lower Mg′), and there was more opportunity (slower cooling) for olivine phenocrysts and melt to react.

Computational crystallization models for 12009 calculated by MELTS approach those of experimental crystallization studies. In the computational equilibrium and fractional crystallization model for 12009, spinel is the first phase to crystallize at 1273 °C and is followed by olivine (Fo$_{76}$) at 1263 °C. Experimental studies by Green et al. (1971) showed that olivine (Fo$_{75}$) was the first liquidus phase at approximately 1230 °C and was followed rather than preceded by spinel. In the computational results, low-calcium pyroxene crystallized at 1190 °C after 10% olivine crystallization. In the fractional crystallization model, crystallization of olivine (Fo$_{71}$) terminated once pyroxene became the liquidus phase. In the equilibrium crystallization model, olivine reacted with the melt
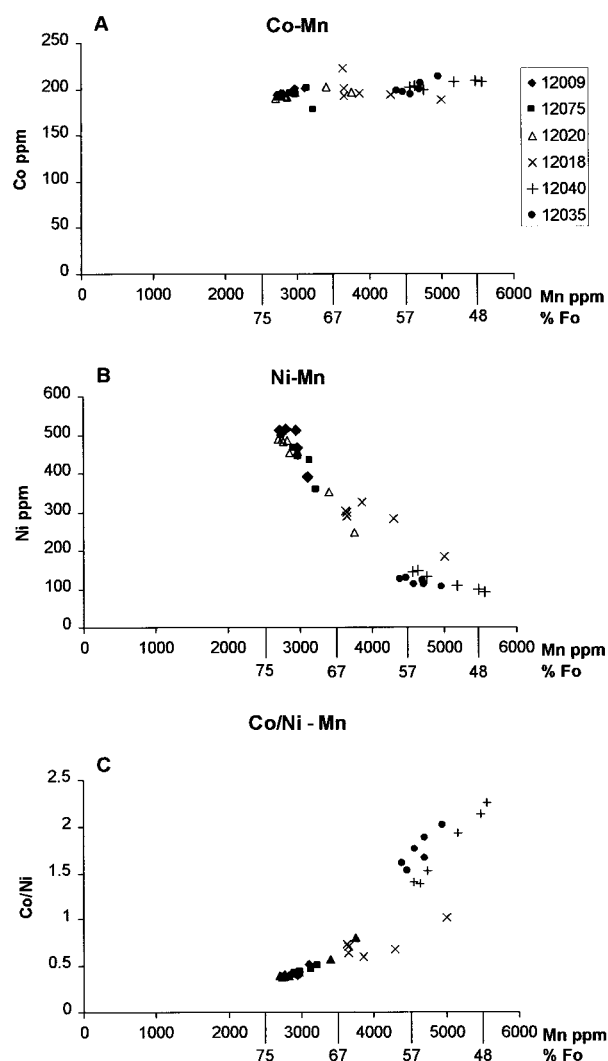
to produce pyroxene. During this reaction, the abundance of olivine decreases and reaches a composition of Fo$_{58}$ upon the crystallization of plagioclase at approximately 1133 °C. Plagioclase became a liquidus phase after 46% of 12009 had crystallized. Experimental results indicate that pigeonite becomes a liquidus phase at 1190 °C as a result of an olivine-consuming reaction. Plagioclase starts to crystallize at 1040 °C. The olivine composition when plagioclase starts to crystallize in the experimental runs is Fo$_{55}$ (Green et al. 1971). The relationship among phases in sample 12009 are obscured because it chilled rapidly from 1190 °C and did not precipitate pyroxene or plagioclase.

Using the melt compositions, sequence of crystallization, and proportion of solids from MELTS, we calculated the fractional and equilibrium trajectories for Ni and Co during olivine crystallization. Figure 6 compares the cal-
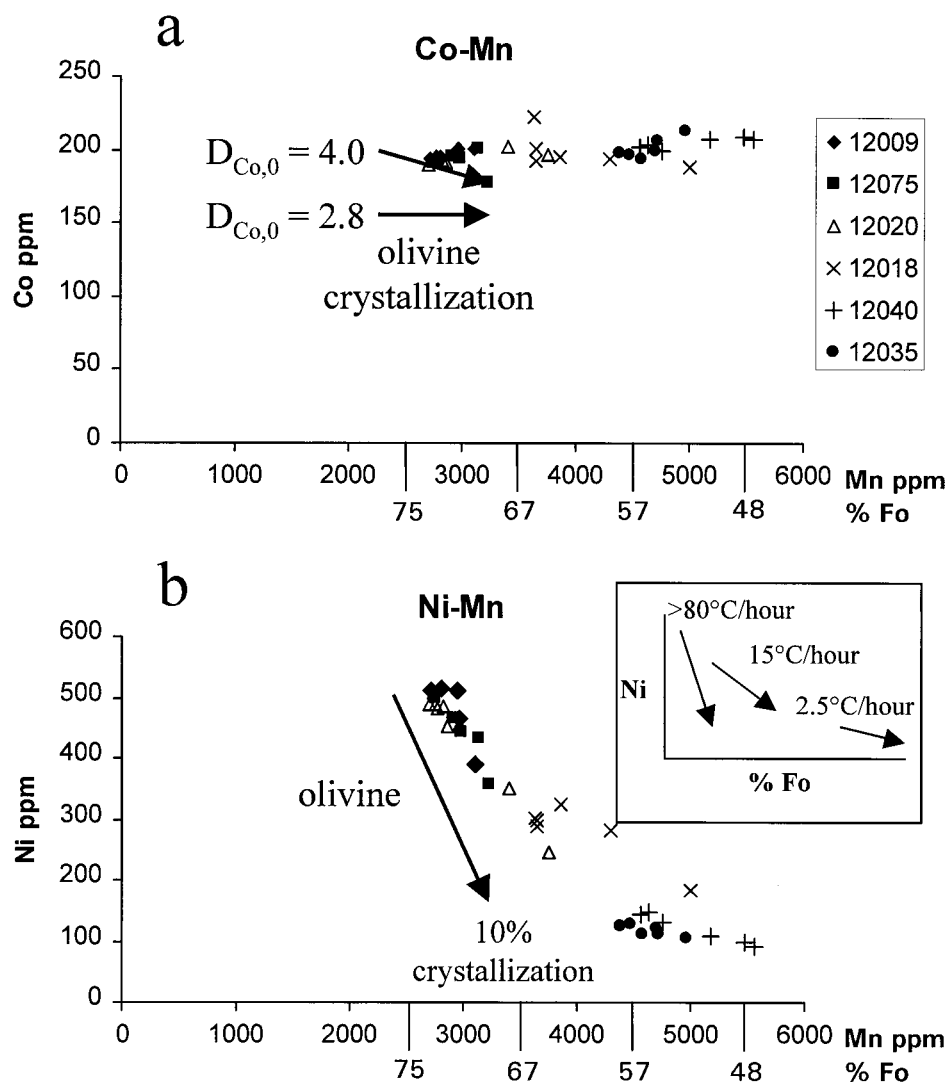
FIGURE 6. (**a**) Variation in Co and Fo in olivine from Apollo 12 olivine basalts compared to calculated trajectories for olivine. Two different sets of D values were used to calculate trajectories to illustrate the balance between D and melt composition in controlling the Co concentration in the olivine. (**b**) Variation in Ni and Fo in olivine from Apollo 12 olivine basalts (Fig. 5) compared to calculated trajectories for olivine. The set of D values illustrated in Figure 3 were used in these calculations. The inset represents the change in slope with cooling rate. This is not a result of changing D values for Mg and Ni, but reflects the anticipated extent of reequilibration due to slower cooling rate.

culated percentage of Fo and Ni concentration in olivine with the measured values for the Apollo 12 olivine basalts. As expected from D values significantly greater than 1, the calculated Ni exhibits a substantial decrease over a very limited range of Fo percent and degree of crystallization (10%). Fractional and equilibrium crystallization are fairly similar. As illustrated in Figure 6, the steep slope calculated corresponds with data for the most rapidly cooled Apollo 12 olivine basalts. More slowly cooled basalts have more time for olivine-melt reequilibration, and data arrays for these basalts have different slopes (Fig. 6, inset).

In contrast to Ni, the measured and calculated concentrations of Co in the olivine exhibit limited variation over a wide range of Fo percent (Fig. 6). This fairly flat pattern for Co variation reflects the interplay between changing $D_{Co}^{olivine}$ and Co content in the melt. At fairly low D values (but still >1), slight increases in D with decreasing MgO of the melt will result in a balance between the decreasing concentrations of Co in the melt and the preference for Co in olivine. Only slightly higher D values for Co (D_{Co_2}) will not produce this effect. This relationship is illustrated better in Figure 7. During olivine crystallization, both Co and Ni concentrations should decrease in the melt (Fig. 7a). Due to its greater compatibility in olivine, Ni should exhibit a substantial decrease in the melt

REFERENCES CITED

BVSP (Basaltic Volcanism Study Project) (1981) Basaltic volcanism on the terrestrial planets, 1286 p. Pergamon Press, New York.

Donaldson, C.H., Usselman, T.M., Williams, R.J., and Lofgren, G.E. (1975) Experimental modeling of the cooling history of Apollo 12 olivine basalts. Proceedings of the 6th Lunar Science Conference, 843–869.

Ghiorso, M.S. and Sack, R.O. (1995) Chemical mass transfer in magmatic processes IV. A revised and internally consistent thermodynamic model for the interpolation and extrapolation of liquid-solid equilibria in magmatic systems at elevated temperature and pressures. Contributions to Mineralogy and Petrology, 119, 197–212.

Green, D.H., Ware, N.G., Hibberson, W.O., and Major, A. (1971) Experimental petrology of Apollo 12 basalts. Part 1, Sample 12009. Earth and Planetary Science Letters, 13, 85–96.

Hart, S.R. and Davis, K. (1978) Nickel partitioning between olivine and silicate melt. Earth and Planetary Science Letters, 40, 203–219.

Jones, J.H. (1995) Experimental trace element partitioning. In rock physics and phase relations, a handbook of physical constants, A.G.U. References Shelf 3. American Geophysical Union, 73–104.

Kinzler, R.J., Grove, T.L., and Recca, S.I. (1990) An experimental study on the effect of temperature and melt composition on the partitioning of nickel between olivine and silicate melt. Geochimica et Cosmochimica Acta, 54, 1255–1265.

Kohn, S.C., Henderson, C.M.B., and Mason, R.A. (1989) Element zoning trends in olivine phenocrysts from a supposed primary high-magnesian andesite: an electron- and ion-microprobe study. Contributions to Mineralogy and Petrology, 103, 242–252.

Lofgren, G.E. and Lofgren, E.M. (1981) Catalog of lunar mare basalts greater than 40 grams. Part 1. Major and trace chemistry. Lunar and Planetary Institute Contribution no. 438, 418 p.

Miyamoto, M. and Takeda, H. (1983)Atomic diffusion coefficients calculated for transition metals in olivine. Nature, 306, 602–603.

Morioka, M. (1980) Cation diffusion in olivine: I. Cobalt and magnesium. Geochimica et Cosmochimica Acta, 44, 759–762.

———(1981) Cation diffusion in olivine: II. Ni-Mg, Mn-Mg, Mg and Ca. Geochimica et Cosmochimica Acta, 45, 1573–1580.

Neal, C.R., Hacker, M.D., Snyder, G.A., Taylor, L.A., Liu, Y.G., and Schmitt, R.A. (1994a) Basalt generation at the Apollo 12 site, Part 1: New data, classification, and revaluation. Meteoritics, 29, 334–348.

———(1994b) Basalt generation at the Apollo 12 site, Part 2: Source heterogeneity, multiple melts, and crustal contamination. Meteoritics, 29, 349–361.

Papike, J.J., Hodges, F.N., Bence, A.E., Cameron, M., and Rhodes, J.M. (1976) Mare basalts: crystal chemistry, mineralogy, and petrology. Reviews of Geophysics and Space Physics, 14, 475–540.

Papike, J.J., Spilde, M.N., Fowler, G.W., Layne, G.D., and Shearer, C.K. (1995) The Lodran primitive achondrite: Petrogenetic insights from electron and ion microprobe analysis of olivine and orthopryoxene. Geochimica et Cosmochimica Acta, 59, 3061–3070.

Shimizu, N., Semet, M.P., and Allégre, C.J. (1978) Geochemical applications of quantitative ion-microprobe analysis. Geochimica et Cosmochimica Acta, 42, 1321–1334.

Walker, D., Kirkpatrick, R.J., Longhi, J., and Hays, J.F. (1976a) Crystallization history of lunar picritic basalt Sample 12002: Phase-equilibria and cooling-rate studies. Geological Society of America Bulletin, 87, 646–656.

Walker, D., Longhi, J., Kirkpatrick, R.J., and Hays, J.F. (1976b) Differentiation of an Apollo 12 Picrite Magma. Proceedings of the 7th Lunar Science Conference, 1365–1389.

FIGURE 7. Calculated Mg′, Ni, and Co in melt (**a**) and olivine (**b**) during the crystallization of a 12009 bulk composition. The crystallization sequence calculated from MELTS is superimposed on (**a**). The range in Mg′ in **a** is larger than in **b**. In **b**, open circles represent Co in olivine assuming $D_{Co} = 2.8$, whereas open squares represent Co in olivine assuming $D_{Co} = 4.0$. The variations of D values illustrated in Figure 3 were used in these calculations.

(52 ppm → 16 ppm) compared to Co (49 ppm → 38 ppm). With the limited decrease in Co in the melt, the increasing D should result in the Co concentration in olivine exhibiting limited variation (Fig. 7b).